Journal of Innovative Optical Health Sciences
Vol. 4, No. 2 (2011) 97−111

DOI: 10.1142/S1793545811001460

World Scientific
www.worldscientific.com

OPTICAL MEASUREMENT OF PHOTOSENSITIZER CONCENTRATION *IN VIVO*

MARTIN R. AUSTWICK*, JOSEPHINE H. WOODHAMS*,‡, VADZIM CHALAU*, CHARLES A. MOSSE*, CAROLINE ELIOT*, LAURENCE LOVAT*, ALEXANDER J. MACROBERT*, IRVING J. BIGIO† and STEPHEN G. BOWN*

*National Medical Laser Centre
Charles Bell House, 67-73 Riding House Street
University College London
London W1W 7EJ, UK

†Boston University, BME, 44 Cummington Street
Boston, MA 02215, USA
‡j.woodhams@ucl.ac.uk

Most techniques for measuring tissue concentrations of drugs are invasive, time-consuming, and often require the removal of tissue or body fluids. Optical pharmacokinetics (OP) is a minimally invasive alternative giving an immediate result. Pulses of white light are directed at the tissue of interest using a fiber optic probe. Scattered light is detected by a second fiber immediately adjacent to the first in the same probe (separation 1.7 mm). Using the photosensitizer disulfonated aluminium phthalocyanine (AlS_2Pc), OP measurements were made in phantoms and on the mouth, stomach, colon, skin, and liver of normal rats 1 and 24 h after intravenous AlS_2Pc administration. AlS_2Pc concentration was determined by calculating the area under the curve (AUC) in the spectral region around the peak drug absorption or measuring the height of the peak. Spectral baseline interpolation removed the need for pre-drug, control optical measurements. OP measurements correlated well with values from alkali chemical extraction (CE) of the corresponding tissues, (R^2 0.87−0.97). OP measurements in the mouth also correlated with CE of less accessible internal organs (R^2 0.77−0.88). In phantoms, the lowest detectable concentration was 0.1 μg/g. *In vivo*, results were limited by the lower accuracy in the CE measurements but were almost certainly comparable. An incidental finding was a 12−15 nm red shifted component in the spectra observed 1 h after drug administration, suggesting partitioning of the drug in different microenvironment compartments, which could prove to be of considerable interest in future studies. In conclusion, OP shows promise for real-time measurement of concentrations of drugs with suitable absorption peaks.

Keywords: Optical pharmacokinetics; chemometrics; photodynamic therapy; noninvasive measurement.

1. Introduction

Most current methods for quantifying drug concentrations in tissue are invasive and usually require tissue extraction, making them unsuitable for real-time dosimetry. An important potential application of optical pharmacokinetics (OP) is for the dosimetry of photosensitizers for photodynamic therapy (PDT). This paper addresses the use of OP, a noninvasive

white-light spectroscopic measurement collected via a fiber-optic probe, for the quantitative monitoring of *in vivo* tissue concentrations of PDT drugs that absorb in the visible (vis) and near infrared (NIR) region.[1] Previous work focused on chemotherapy agents[1,2] and topical photodynamic agents.[3] In this paper, we describe novel applications of the OP method in assessing the concentration of a systemically administered photosensitizer and the correlation between chemical measurements in less-accessible internal organs and OP measurements in a more accessible organ (the mouth).

For very small source-detector separations of fiber-optic probes (<500 microns), in the technique known as elastic scattering spectroscopy (ESS), diagnostic signatures have been shown in a number of disease/organ systems[4–6] and can be used to extract the intrinsic optical properties of the superficial layers.[7] For larger source-detector separations (>4 mm), methods based on the diffusion equation can extract the optical properties, but these methods provide average values for larger tissue volumes, thus lacking site specificity. Also, most systems for doing this are limited to the red and NIR because absorption by water and hemoglobin is too strong at other wavelengths.[8–10] For intermediate source-detector separations, the OP method offers the opportunity for the quantitative measurement of absorption, due to specific chromophore absorption characteristics, enabling greater sensitivity than ESS, while retaining highly localized site-specificity. If the fiber separation is in the range 1.6–2.5 mm, the geometry is such that the effective photon path length is almost insensitive to the (reduced) scattering coefficient of the tissue, μ_s'. The path length is hence independent of morphological changes within the tissue, yet is long enough for sensitive detection of small concentrations of strongly absorbing chromophores.[1–11] This facilitates the use of Beer's law for extraction of the absorption coefficient, independent of scattering properties. Within this range of separations, the depth of sensitivity, as well as the sensitivity to small drug concentrations, increases for larger separations. The optimum separation may be chosen to best suit the thickness of the tissue being sampled. This scattering-independent path length means that the concentration can be extracted in a straightforward fashion. In tissue, the path length is approximately 5 mm and the sampling volume is presumed to be close to 1 mm^3 for this fiber geometry and wavelength range (650–700 nm). In this study, a fiber separation of 1.7 mm was chosen. Other fiber separations were not studied.

PDT is a chemotherapeutic technique used to treat a range of cancerous and pre-cancerous conditions.[12] The patient is administered a photosensitizer (PS) either topically or systemically, and the targeted area is illuminated, usually with laser light. The PS is excited to a chemically active state, which combines with oxygen in the tissue to create cytotoxic species (e.g., singlet oxygen, superoxide), causing local cellular damage whilst typically leaving connective tissue intact. Effective therapy depends on the concentration of photosensitizer, of oxygen, and photoactivating light at every point in the target tissue. A real-time measurement (minimally invasive or noninvasive) of PS concentration in the target region would thus enable more predictable cytotoxicity, assuming available oxygen and light. PS biodistribution, even within a healthy organ, can be markedly heterogeneous, and site-specific measurements can provide valuable information.

The OP technique could be particularly valuable where the PDT is to be carried out interstitially under image guidance[13–15] on an inaccessible organ[16]; if OP were extended to correlate measurements in the mouth (or other accessible organ) with PDT effects in a less-accessible organ, the technique could improve the efficacy of therapy even further.[17] This paper addresses these possibilities with studies using the photosensitizer aluminium disulfonated phthalocyanine (AlS_2Pc), chosen for its stability, solubility, ease of administration, and low toxicity in the absence of light. AlS_2Pc displays a strong, well-defined absorption band around 670–675 nm, with a line width of about 10 nm.[18] Its extinction coefficient at this wavelength reaches 2×10^5 $M^{-1}cm^{-1}$, compared to 3×10^3 $M^{-1}cm^{-1}$ for porfimer sodium (Photofrin) and 3×10^4 $M^{-1}cm^{-1}$ for mTHPC (meso-tetra(hydroxyphenyl)chlorine. Foscan), other PS drugs in clinical use. Even adjusting for the typical molar concentrations used clinically, AlS_2Pc gives a much stronger optical signal, and our group has extensive pre-clinical experience with this PS.[19,20] Work with other phthalocyanines has begun recently in the treatment of cutaneous t-cell lymphoma,[21] and many aspects of our study can be generalized to a variety of agents.

2. Methods and Materials

2.1. *Photosensitizer*

AlS_2Pc powder (Frontier Scientific Ltd., UK) was used to prepare the required concentration for intravenous injection by dissolving 1 mg into 50 μL of 0.1 M sodium hydroxide (Sigma-Aldrich, UK) and then adding phosphate buffered saline (Sigma-Aldrich, UK) to make the required volume.

2.2. *Phantom measurements*

To test the limits of sensitivity of our equipment and examine any path length effects, we prepared optical tissue phantoms using 37 mL Phosphate Buffered Saline (PBS), 2 mL of 20% Intralipid®, and varying quantities (0.01, 0.025, 0.05, 0.1, 0.25, 0.5, 1, 2.5, 5, 10, 25, 50, and 75 μg/mL) of AlS_2Pc. The peak height of the negative-log-ratio to a linear baseline interpolation (described below) was examined. Previous work[1] has estimated the path length-dependence on absorption coefficient μ_a in this geometry, using the expression for the path length L

$$L(\mu_a) = x_0 + x_1 \exp(-\mu_a x_2), \qquad (1)$$

and so the phantom data absorbance A can be fitted using the function

$$A(\mu_a) = C + \mu_a[x_0 + x_1 \exp(-\mu_a x_2)], \qquad (2)$$

where C is a constant that accounts for inadequacies in the baseline fit, which lead to nonzero absorbance measures in the absence of added absorbers. Previously,[1] parameters x_0, x_1, and x_2 were measured as 0.6, 1.3, and 3.57 cm, respectively. Another way to capture this deviation from linearity is to use a power-law fit, where $A(\mu_a) = m(\mu_a)^n$, as utilized in Ref. 2.

2.3. *Animal model*

Wistar rats (180−220 g, Harlan UK Ltd., Blackthorn, Oxfordshire, UK) were housed under diurnal lighting conditions and allowed food and tap water *ad libitum*. Rats were anesthetized with 2% halothane (Merial Animal Health Ltd., Harlow, UK) in oxygen for induction and maintenance throughout surgery, with the animals breathing spontaneously. Analgesia was administered subcutaneously 1 h prior to surgery (Vetergesic®, buprenorphine hydrochloride, Reckitt Benckiser Healthcare Ltd., Hull, UK). All procedures were carried out under the authority of project and personal licences granted by the UK Home Office and the UKCCCR Guidelines (2010).

2.4. *OP measurements on tissues*

Rats were sensitized with dosages of 0 (control animals), 0.1, 0.2, 0.25, 0.5, 1.0, or 2.5 mg/kg of AlS_2Pc as a bolus injection into the tail vein. At 1 or 24 h later (immediately for control animals), OP measurements were performed on shaved abdominal skin, thigh muscle with skin removed, oral mucosa and, after laparotomy, on liver, glandular stomach, and colon. Three rats were used for each drug dose and each time interval; the intervals were chosen to see whether different biodistributions affected the quality of the results. At 1 h, the drug will still have a significant proportion within the vasculature, whereas by 24 h it will reside mainly within the organ parenchyma.[22] The OP fiber-optic probe (described below) was positioned by means of a micromanipulator, so that it was just touching the surface of the organ under examination. On each organ, 10 separate positions were chosen, with 4 OP measurements being taken at each position (i.e., 40 spectra per organ). When only a small thickness of tissue was being investigated, a piece of matt black card was placed under the tissue to minimize the effects of light that passed through the tissue and out the far side, and might be scattered back from other adjacent tissues.

Immediately after the OP measurements were completed, the animals were killed, and the OP measurements were repeated post mortem in the same organs. Tissue samples were collected from each animal and stored at −20°C for alkaline extraction of AlS_2Pc.[20]

2.5. *Alkaline extraction of AlS_2Pc from tissue*

Finely-cut thawed tissue samples, including controls of each organ from unsensitized animals, were added to 0.1 M sodium hydroxide (NaOH, Sigma-Aldrich, UK) at a ratio of 0.1 g into 10 mL NaOH. From each animal, four samples of each organ were processed. The tissues in NaOH were incubated in a water bath at 50°C for 6 h in darkness to allow cell breakdown. The samples were shaken approximately

halfway through the incubation period to ensure adequate breakdown of cell structures to release the AlS_2Pc. AlS_2Pc concentrations in the resulting solution were measured by spectrofluorimetry (Perkin-Elmer LS50 Luminescence Spectrophotometer). The solutions were loaded into 96-well plates, and fluorescence was measured using a Perkin-Elmer LS50 luminescence spectrometer at excitation and emission wavelengths of 605 and 675 nm, respectively. A slit width of 10 nm and an integration time of 1 were set for both excitation and emission. The emission was long-pass filtered to eliminate scattered light at wavelengths shorter than 645 nm (RG645 Schott long-pass filter). The concentration of AlS_2Pc in each specimen could then be calculated against a standard curve. A standard curve was prepared each time a chemical extraction (CE) was undertaken using 0.1 M NaOH solutions with known concentrations of AlS_2Pc. Calibration curves were plotted for three ranges of concentration: 0 to 0.5, 0 to 0.1 and 0 to 0.01 μg/mL; for the liver, in which higher concentrations of drug accrued, a larger-range calibration curve was constructed, covering 0 to 100 μg/mL. A molecular weight of 735.08 g/mol was used for calculations of AlS_2Pc concentrations.

2.6. *OP system*

The OP collection apparatus consists of a light source, delivery and collection fibers, a spectrometer, and a laptop computer, see Fig. 1. OP data were collected from tissues using a pair of fibers inside a catheter. The tip of the catheter was positioned to be just touching the tissues to be interrogated and, at the tip, the fiber centers were 1.7 mm apart, which

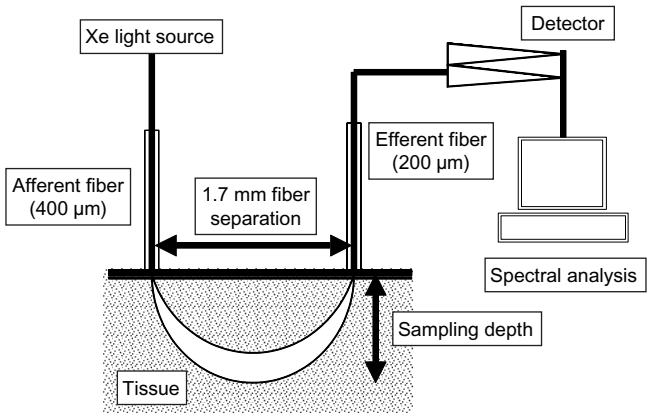

Fig. 1. Schematic diagram of the Optical Pharmacokinetic system.

was chosen on the basis of previous publications as discussed in Sec. 1. The light from a pulsed Xenon arc lamp (model LS1130/FX1100, Perkin Elmer Optoelectronics) was delivered using a 400-μm core, vis/NIR fiber and the light scattered back was collected with a 200-μm core, vis/NIR fiber connected to a spectrometer (model S2000, Ocean Optics, Inc.). Before each experiment the system was calibrated using a reference spectrum collected from white Spectralon® (Labsphere, NH, USA), a spectrally flat diffuse-reflecting polymer. For each measurement, ambient light was collected immediately before the (lamp-illuminated) measurement and subtracted from the signal. The tissue spectrum $[I_{\text{raw}}(\lambda)]$ and Spectralon® reference spectrum $[I_{\text{ref}}(\lambda)]$ were smoothed using a seven-point ($\sim$3 nm) moving-window average, and the tissue spectrum was divided by the reference spectrum to provide a spectrum that could be calibrated for system response.

$$I(\lambda) = I_{\text{raw}}(\lambda)/I_{\text{ref}}(\lambda). \tag{3}$$

2.6.1. *OP spectral analysis*

If $A(\lambda)$ is the signal attenuation, the Beer–Lambert law states

$$I_{\text{raw}}(\lambda) = I_0(\lambda)10^{-A(\lambda)}, \tag{4}$$

where $I_0(\lambda)$ represents the spectral output of the light source modified by the system response (detector, transfer optics, etc.), and can then be given (within a scaling factor) by $I_0(\lambda) = I_{\text{ref}}(\lambda)$. Inserting this into Eq. (4) gives

$$I(\lambda) = 10^{-A(\lambda)}. \tag{5}$$

We can further split $A(\lambda)$ into photosensitizer and tissue components

$$A(\lambda) = A_{\text{PS}}(\lambda) + A_{\text{tissue}}(\lambda). \tag{6}$$

The tissue attenuation A_{tissue} will include tissue absorption and scattering, in particular the effects of (oxyhemoglobin (HbO) and deoxyhemoglobin (Hb)). From Eqs. (5) and (6)

$$\begin{aligned} A_{\text{PS}}(\lambda) &= A(\lambda) - A_{\text{tissue}}(\lambda) \\ &= -(\log_{10}[I(\lambda)] - \log_{10}[I_{\text{tissue}}(\lambda)]) \end{aligned} \tag{7}$$

$$\langle L\rangle c_{\text{PS}}\alpha_{[\text{PS}]} \approx -\log_{10}\left[\frac{I(\lambda)}{I_{\text{tissue}}(\lambda)}\right], \tag{8}$$

where c_{PS} is the photosensitizer concentration, $\langle L \rangle$ is the effective mean photon path length, and $\alpha_{[PS]}(\lambda)$ is the extinction coefficient of the photosensitizer. Our OP measure will be based on the quantity A_{PS} (see below).

If it were necessary to take baseline optical measurements in difficult-to-reach sites prior to drug administration, this would limit the clinical use of the technique in some clinical applications, and even when such a measurement is possible, time variation of the tissue properties and errors in co-registration mean that the tissue component will not be completely removed from the spectrum by the process. It is therefore desirable to use methods to estimate the tissue contribution from spectra taken from sensitized animals, without the need for a reference spectrum from an unsensitized animal.

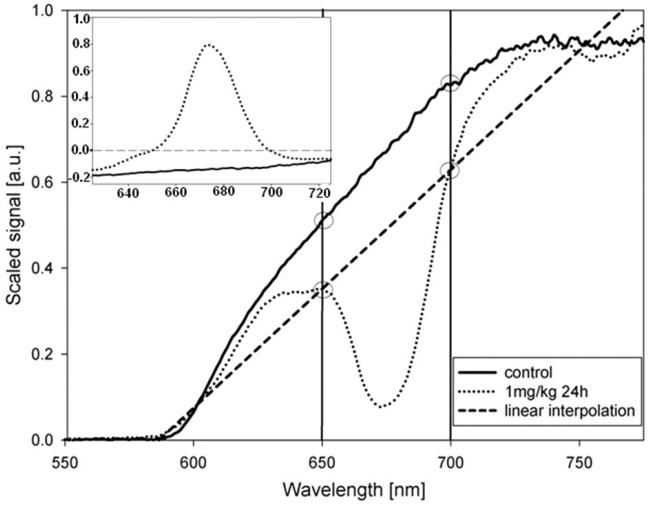

Fig. 2. Linear interpolation of OP data (taken from the liver). Inset shows negative $\log_{10}$ ratio of data and linear interpolation.

2.6.2. *Optical pharmacokinetic metrics*

In this study, the OP metrics we considered to measure the drug absorption were AUC*, AUC,† and peak-fitting metrics (A_1 and A_2). Area-under-curve (AUC) methods (AUC* and AUC†) calculate the area under a peak over a specified wavelength range, which inherently incorporates some noise-averaging. Each AUC technique used a different method for baseline removal, detailed below. Finally, a peak-fitting method was tried, which uses aqueous AlS_2Pc spectra to fit to animal data; this should account for any spectrally shifted (but not broadened or otherwise modified) components in the *in vivo* drug spectrum, but is more analytically complex. These approaches are detailed below.

The absorption feature of interest in the AlS_2Pc spectrum is the strong peak at 672 nm.[23] The tissue absorption at these wavelengths can be estimated by linear interpolation of the spectrum between two points (650−700 nm), shown in Fig. 2. We call this function $I_{linear}(\lambda)$. In this range we expect the baseline to be smooth but not linear, so we would expect a finite (positive or negative) area, even for zero AlS_2Pc. We define

$$A^*(\lambda) = -\log_{10}\left[\frac{I(\lambda)}{I_{linear}(\lambda)}\right]. \qquad (9)$$

We use an area under curve measure, AUC*, defined as:

$$\mathrm{AUC}^* \stackrel{\mathrm{def}}{=} \int_{650\ \mathrm{nm}}^{700\ \mathrm{nm}} d\lambda A^*(\lambda). \qquad (10)$$

These limits lie within the full width of the drug peak, chosen in order to capture the local baseline and any possible wavelength shifts and to sample a fixed proportion of the drug absorption peak. Choosing wider limits would mean modulations in the baseline nonlocal to the central drug peak, which could distort the interpolation of the local baseline. Outlier points [points over three standard deviations (SDs) from the animal mean] were iteratively removed.

2.6.3. *Control animals and hemoglobin spectrum removal*

Ratioing spectral data against a characteristic spectrum of the same organ from unsensitized animals was carried out to remove a large proportion of the baseline features common to all animals. An average was formed over five control animals (10 sites per organ, four measurements per site) for each organ to produce the characteristic spectra. Spectra from AlS_2Pc sensitized animals could then be divided by this spectrum, and the negative logarithm taken to give the control-ratio-log (CRL) attenuation

$$A_{CRL}(\lambda) = -\log_{10}\left[\frac{I(\lambda)}{I_{control}(\lambda)}\right]. \qquad (11)$$

The features present in $A_{CRL}(\lambda)$ will be due to differences between the control animal and the sensitized animal. This will include changes in the

hemoglobin saturation and perfusion, the drug signal, and to a less significant extent, in absorption and scattering due to other effects. Oxyhemoglobin (HbO) and deoxyhemoglobin (Hb), the largest contributors to absorption changes, were fitted to $A_{\mathrm{CRL}}(\lambda)$ using spectral Hb/HbO extinction coefficients ($\varepsilon_{\mathrm{HbO/Hb}}$), with ΔC_{HbO} and ΔC_{Hb} as fitting parameters, representing changes in concentration of HbO and Hb (and a constant offset κ to compensate for any changes in intensity of the raw spectra). The hemoglobin extinction coefficients, both HBO and Hb were taken from the Oregon Medical Laser Centre website.[24]

$$A_{\mathrm{fit}}(\lambda) = \Delta C_{\mathrm{HbO}}\varepsilon_{\mathrm{HbO}}(\lambda) + \Delta C_{\mathrm{Hb}}\varepsilon_{\mathrm{Hb}}(\lambda) + \kappa. \quad (12)$$

This fit was carried out in Matlab using their standard curve-fitting toolbox which utilizes a Levenberg−Marquardt approach. The hemoglobin-fit region (520−600 nm and 750−900 nm) was set outside the AlS_2Pc absorption peak. The resulting fit was subtracted from the data to leave a residual spectrum. This was interpolated from 625 to 725 nm, and the line was subtracted to remove any linear baseline remaining (from scatter and any other chromophores). The remaining spectrum, $A^{\dagger}(\lambda)$, was integrated to give

$$\mathrm{AUC}^{\dagger} \stackrel{\mathrm{def}}{=} \int_{650\ \mathrm{nm}}^{700\ \mathrm{nm}} d\lambda A^{\dagger}(\lambda). \quad (13)$$

2.6.4. *Peak position and line shape*

There were variations in both the line shape and in the peak absorption wavelength of the measured drug. Suspecting that this might be due to a chemical shift, we attempted to fit the observed absorption, A^{*} with the function

$$A^{*}_{\mathrm{fit}}(\lambda) = A_1\mathrm{Pth}(\lambda - \lambda_1) + A_2\mathrm{Pth}(\lambda - \lambda_2) + \alpha_0 + \alpha_1\lambda + \alpha_2\lambda^2, \quad (14)$$

where $\mathrm{Pth}(\lambda)$ is the aqueous AlS_2Pc spectrum and λ_n is a factor shifting the central wavelength of the AlS_2Pc peak. The α_n terms represent a local baseline, due to tissue absorption and scattering effects (an attempt was made to fit this baseline with hemoglobin extinction coefficients, but did not provide an accurate or as general a fit). A_1 and A_2 are the contribution from each peak. Figure 3 shows data taken from the colon and fitted using this method. One

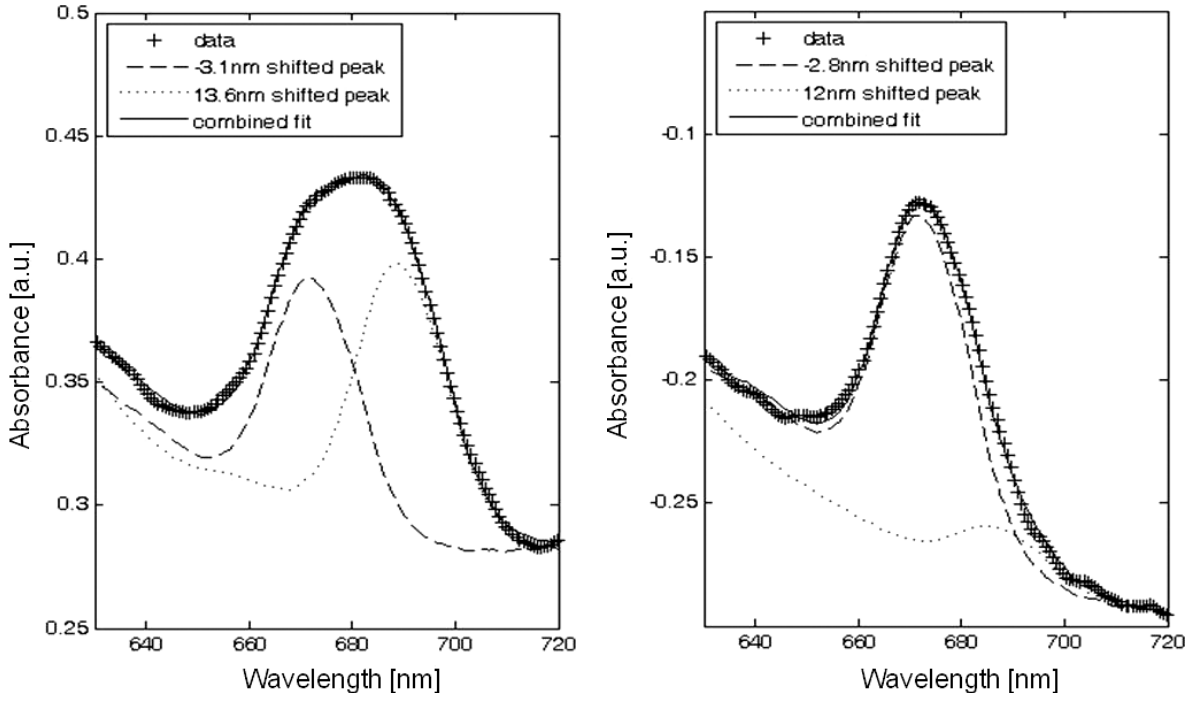

(a) (b)

Fig. 3. Sample colon data showing shifted Phthalocyanine signals at: (a) 1 h, and (b) 24 h.

peak is typically blue-shifted by 0−5 nm, and the other red-shifted by 12−15 nm. Similar results have been reported elsewhere[25] and this will be covered in more detail in the discussion.

Because the line width of each peak did not appear to change, the quantities A_1 and A_2 can be combined to give a measure of total drug concentration, A_{12}:

$$A_{12} = A_1 + A_2. \quad (15)$$

Note that the effects of wavelength-dependent line width changes are not explicitly incorporated, although the baseline-fit might be expected to compensate for this to some degree.

3. Results

3.1. *Phantom study*

The results are shown in Fig. 4, where the absorbance signal of AlS_2Pc is significant and well-separated above 0.1 μg/mL, with an s/n ratio of >10. We were unable to reproduce the path length parameters produced in Ref. 1, and these parameters exhibited sensitivity to the concentration range considered. In part, this is due to aggregation effects of AlS_2Pc, so we constrained our concentration range to typical physiological values for the majority of organs. Confining ourselves to the 0−5 mg/kg range yields $x_0 = 0.38$ cm, $x_1 = 0.38$ cm, and $x_2 = 2.47$ cm. In this spectral region, hemoglobin contributes an absorption baseline of $\sim$0.5 cm^{-1}, giving a baseline path length of $\sim$0.5 cm. 5 mg/kg of AlS_2Pc results in a total μ_a of approximately 2 cm^{-1} and a path length reduction to $\sim$0.4 cm, a 20% decrease in path length from baseline; which would result in a commensurate 20% absorbance reduction. Fitting this relationship with a power law over the same region, following Ref. 2, gave a power of 0.75.

3.2. *Tissue measurements*

Figure 5 shows the correlation between the OP AUC* and CE measurements for colon, skin, muscle, mouth, and stomach. At moderate AlS_2Pc concentrations, there are strong correlations between CE and OP in most organs at 1 and 24 h (Table 1). The correlation is well-described by a linear regression, passing close to the origin — this suggests little zero-point error is introduced by using a linear baseline interpolation. Fitting this relationship using power-law functions proved problematic. Data from the muscle, skin and stomach gave power coefficients greater than or equal to 1, i.e., the fit converged to a linear function, or gave nonphysical results (see discussion). The mouth and colon showed slightly improved fits when a power law was applied; for 1 h, 24 h and all data categories together, the colon exhibited powers of 0.8, 1.2 and 0.6, respectively; and the mouth 0.6, 1.3 and 0.7; clearly the 24 h data is not giving a physical fit to the data.

Figure 6 shows both measures, $A_1 + A_2$, from the peak-fitting function, expected to cover all drug environments. The colon and the mouth alone display a power-law-like behavior, and so power-law fits are included. The powers for the colon (for 1 h, 24 h, and all times together) are 0.7, 1.06, and 0.6. For the mouth, the power coefficients are 0.6, 1.0, and 0.65. For the other organs, these coefficients approached or exceeded unity.

Table 1 summarizes the data correlating OP measurements with CE using AUC*, AUC†, and $A_1 + A_2$, and the correlation of AUC* in the mouth with CE in different organs within the same animal. 1 and 24 h data are shown separately (as AlS_2Pc may have different biodistributions at these times) and together (all data points, not grouped by time). The results using AUC* and AUC† were almost identical. Similarly, the OP results from post-mortem versus (alive) *in vivo* tissues showed close similarity (data not shown), with R^2 values >0.9 being typical for correlations between the two.

One of the aims of this project was to make measurements in an easily accessible organ like the mouth to quantify drug levels in less accessible organs like the stomach. This is illustrated in Fig. 5(f), which correlates CE in the stomach with OP AlS_2Pc signals in the mouth. Table 1 summarizes these correlations between measurements in the mouth with those in the range of organs studied. The liver data shows relatively weak correlation, but the other organs have $R^2 > 0.75$ at 1 h. At 24 h, the correlation is low in the muscle (possibly due to low drug levels in that organ), but with $R^2 > 0.8$ for all others.

In the liver, much higher AlS_2Pc concentrations are seen compared with the other organs. The low OP values documented 1 h after AlS_2Pc administration are probably due to the exceptionally high drug concentration at this time causing shadowing and dimerization (see discussion). Figure 7 shows how poorly the extinction coefficient method correlates for the liver, due to these effects.

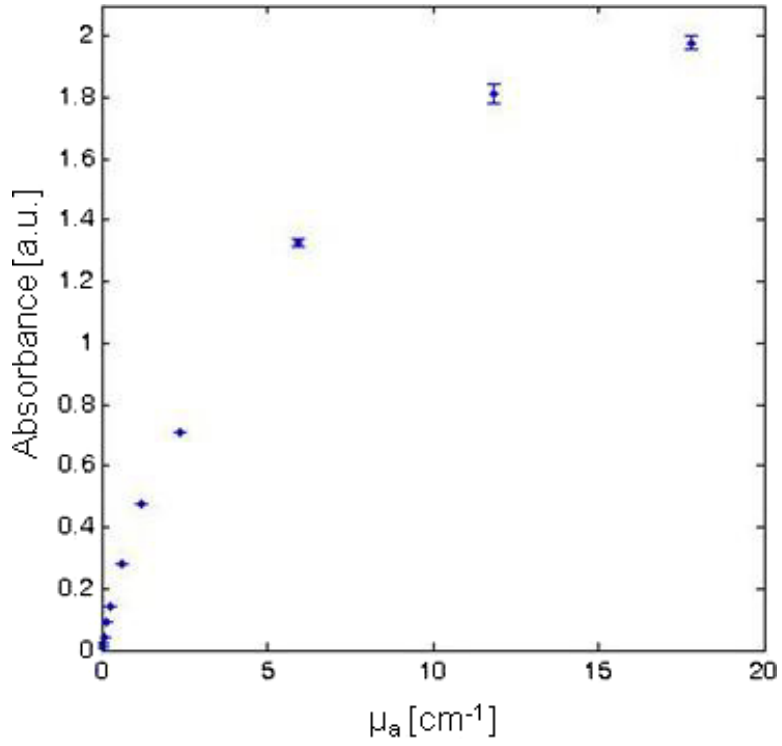

(a)

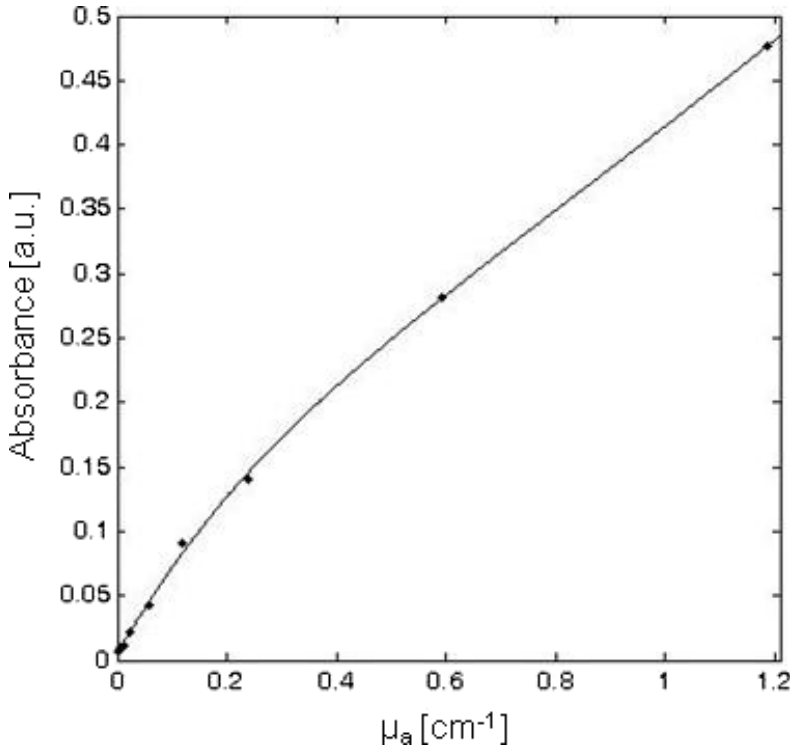

(b)

Fig. 4. OP measures taken on Phosphate Buffered Saline/Intralipid phantoms, plotted against the known absorption at the drug peak. The phantoms were composed of 38 mL PBS and 2 mL of 20% Intralipid®, plus varying amounts of phthalocyanine; (a) shows the full concentration range, and (b) shows the typical physiological range with an exponential path length function fitted to the data (see text).

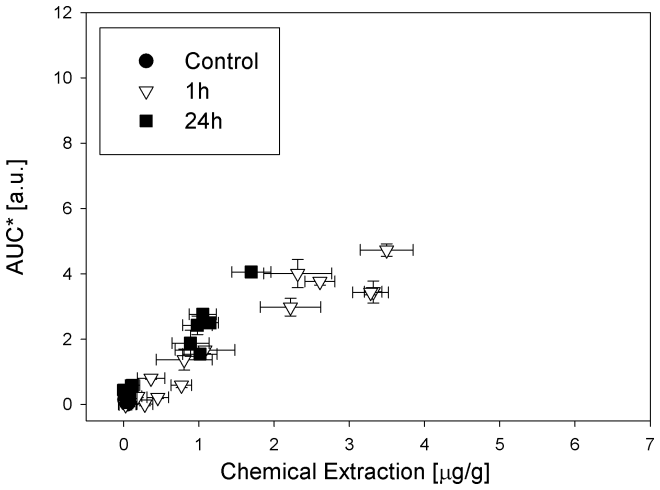

(a) Colon

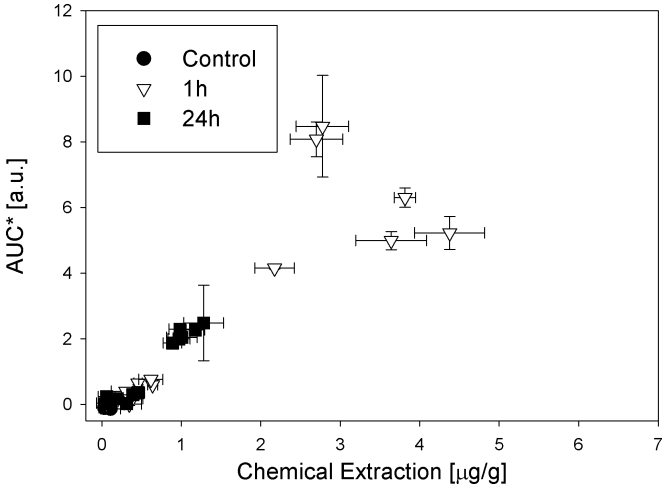

(b) Mouth

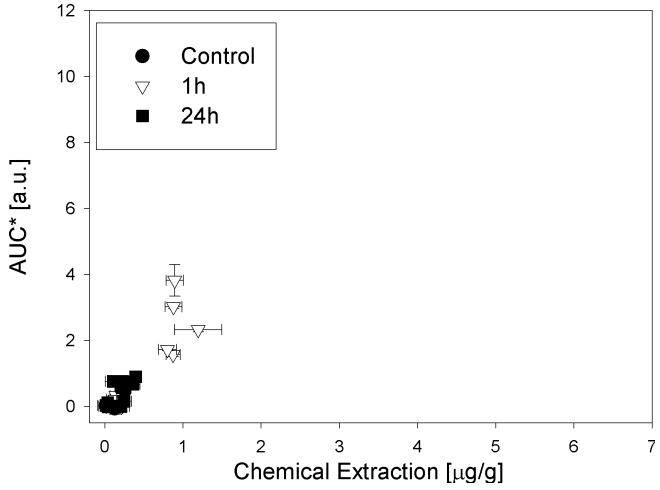

(c) Muscle

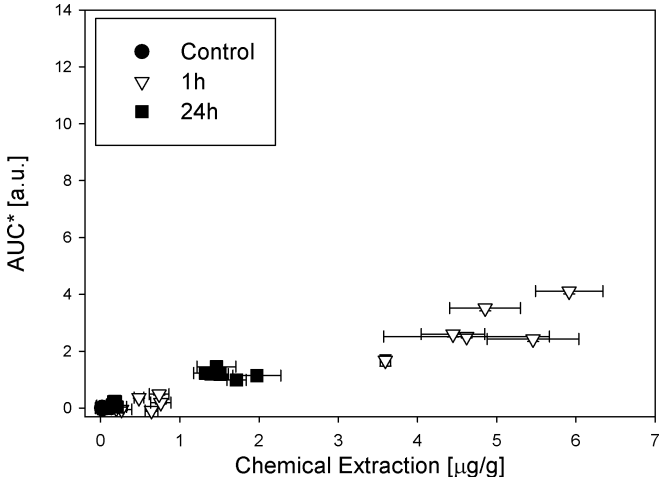

(d) Skin

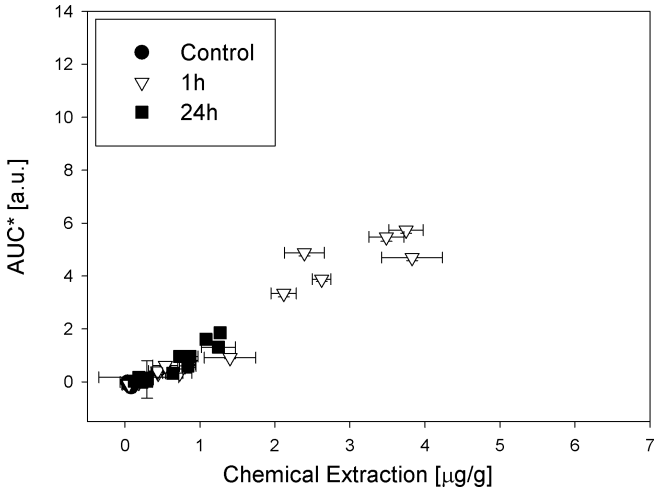

(e) Stomach

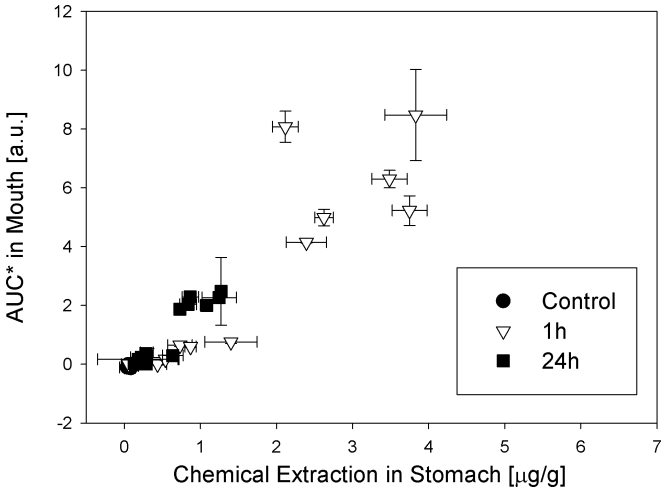

(f) Stomach ce vs AUC* in mouth

Fig. 5. AUC* data versus Chemical Extraction for all organs except liver, which is shown on different scale in Figs. 7. (a)–(e) correlate AUC* with Chemical Extraction in individual organs, (f) correlates CE in the stomach with AUC* in the mouth.

Table 1. R^2 values for OP-CE correlation, including correlation of CE in each organ with AUC* measured in the mouth. R^2 values for fits undertaken with a power-law model are shown in parentheses — the power parameter is stated in the text.

	Colon			Liver			Mouth			Muscle			Skin			Stomach		
	1 h	24 h	all	1 h	24 h	all	1 h	24 h	all	1 h	24 h	all	1 h	24 h	all	1 h	24 h	all
AUC* R^2	0.93 (0.94)	0.95 (0.96)	0.84 (0.88)	0.57	0.97	0.82	0.77 (0.82)	0.96 (0.96)	0.79 (0.83)	0.87	0.49	0.83	0.94	0.92	0.91	0.94	0.92	0.95
AUC† R^2	0.91	0.95	0.87	0.56	0.95	0.82	0.81	0.95	0.84	0.89	0.58	0.86	0.94	0.91	0.94	0.95	0.87	0.94
$A_1 + A_2$ R^2	0.92 (0.93)	0.94 (0.94)	0.87 (0.91)	—	—	—	0.80 (0.84)	0.91 (0.93)	0.82 (0.82)	0.85	0.14	0.79	0.91	0.76	0.88	0.91	0.60	0.90
AUC* R^2 (vs OP in mouth)	0.77	0.94	0.79	0.36	0.82	0.27	—	—	—	0.86	0.45	0.82	0.79	0.95	0.81	0.81	0.88	0.82

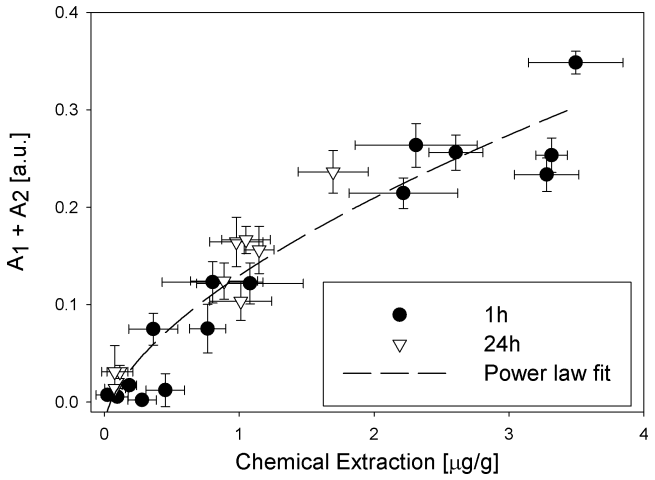

(a) Colon

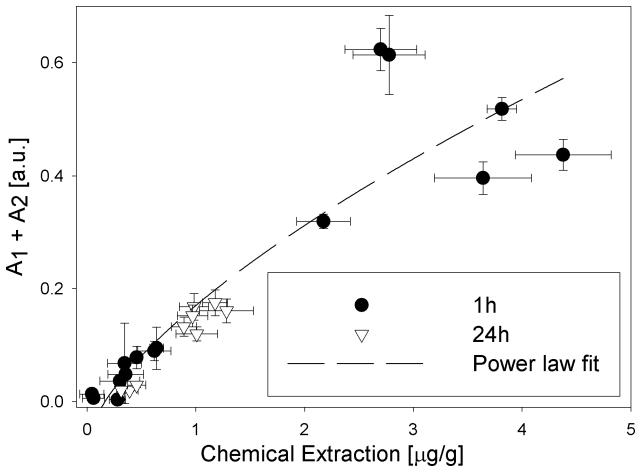

(b) Mouth

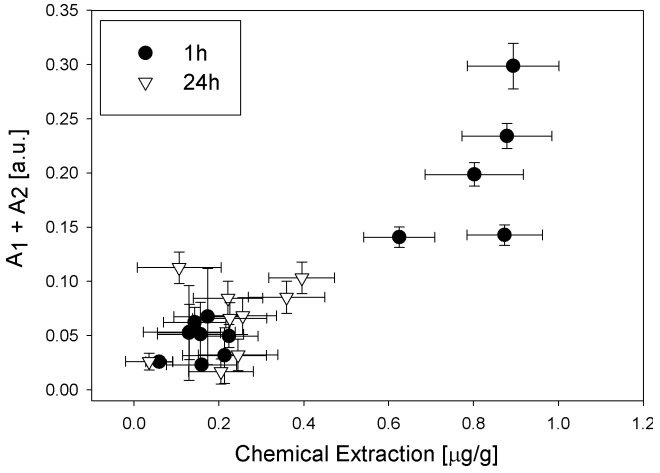

(c) Muscle

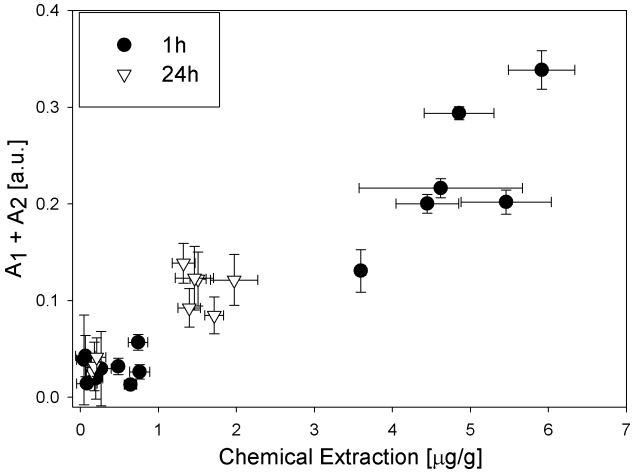

(d) Skin

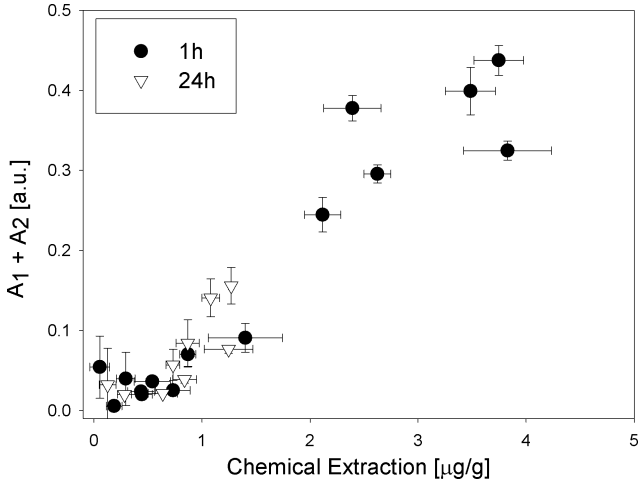

(e) Stomach

Fig. 6. $A_1 + A_2$ versus Chemical Extraction for all organs except liver. Note that each graph is on a different scale for readability. Colon and mouth have power-law regression plotted.

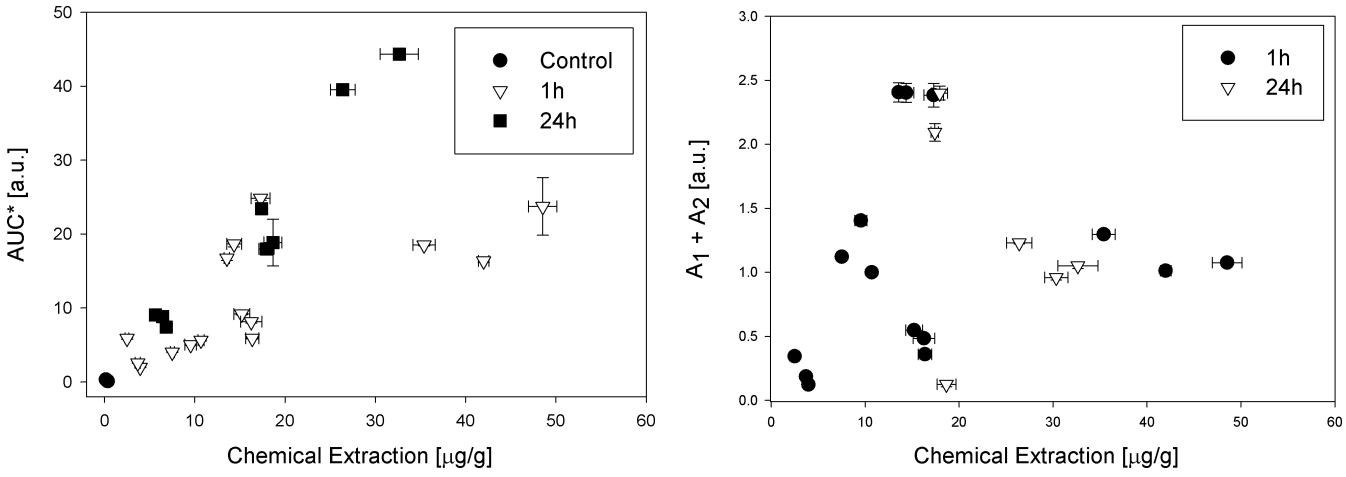

(a) AUC* (b) A_{12}

Fig. 7. (a) AUC* versus Chemical Extraction for liver. (b) A_{12} versus Chemical Extraction for liver. Poor correlation in the curve-fitting method may be due to dimerization.

4. Discussion

4.1. *Chemical extraction — OP correlation*

One of our aims was to determine whether Optical Pharmacokinetics could be used as a minimally invasive technique to measure the concentration of photodynamically active drugs, photosensitizers, *in vivo* in real time, with a particular emphasis on estimating the level of photosensitizers in target tissues at the time of light delivery for PDT. The OP technique has proven successful in phantom measurements, where OP can comfortably detect drug at 0.1 μg/g (100 ng/g), but the *in vivo* situation proved to be more complicated. The uncertainty inherent in the Chemical Extraction measurements is at least 0.1 μg/g, giving a lower limit of quantitation (LLQ) of at least 0.3 μg/g; the uncertainty in each AUC* measurement is of order 0.01 μg/g, but the statistical scatter about the line of best fit is somewhat larger.

At larger concentrations, as measured by CE, the variance can be extremely large (residuals > 1 μg/g), and even at the lowest values, CE gives a variance of typically 0.1−0.3 μg/g. However, because this is similar to the absolute value, it is difficult to place a LLQ on the *in vivo* OP measurements based on the CE data. It appears the variance within individual OP sites is a factor of 10 lower than the CE measure, and the scatter about the line of best fit is similar in magnitude to the error in the CE measure, implying substantial variation between individual measurement sites within organs. To fully test the LLQ sensitivity of OP, it will be necessary to improve the sensitivity of CE by at least a factor of 10. This could be achieved following recent improvements in the technique, such as using the Solvable^{TM} (Perkin Elmer) Chemical Extraction medium, which typically requires five times less solvent (increasing signal fivefold)[26] and more sensitive fluorimeters. Alternatively, either taking measurements using cuvettes or photon-counting detectors would significantly improve the sensitivity of the assay, but would increase the collection time and cost, respectively. The method of HPLC utilized by other researchers (for example, Ref. 2) is extremely sensitive (drug concentration as low as 0.03 μM) and would provide another alternative. Unfortunately, we did not have access to such equipment.

Phantom measurements showed a nonlinear OP/concentration curve, indicative of the absorption dependence of the path length. While previous studies[1,2] show a similar nonlinear behavior, the parameters we extracted from our measurements were somewhat different to those previously reported; for example Mourant *et al.*, 1999[1] used a much smaller range of drug concentrations than ourselves; we were able to observe a strong concentration-dependence of the path length-fitting parameters.

For the majority of the *in vivo* data, power-law fits provide no fitting advantage, and in many cases utilize a power coefficient $\sim$1, or even worse, $>$1; this case predicts an *increasing* path length with

increasing absorption, and can be interpreted as a fitting artefact due to large statistical scatter in the dataset. This can also be ascribed to inter- and intra-animal variations. Based on our phantom measurements, a tissue absorption baseline into which 5 μg/g of AlS_2Pc is introduced will result in a 20% reduction in signal; the other sources of variance and uncertainty at present dwarf this change, explaining why the nonlinearity of the fit is not well-pronounced in much of the data.

At high concentrations, one must consider dimerization, where two AlS_2Pc molecules are weakly bound together; the resulting organic complex has a broader, weaker extinction coefficient (reported as a feature centered around 670 nm with a full width half maximum in excess of 100 nm[18,23]). The CE process ensures that any AlS_2Pc is fully monomerized at the time of the fluorescence measurement, giving a measure of the total AlS_2Pc, but *in vivo* dimerization will mean that the OP AUC* integral will not be an accurate reflection of the total drug concentration. The dimer form is significantly less active in photodynamic therapy,[18] so it may be beneficial that OP preferentially detects the main photoactive component. However the situation is complex as there is also evidence that the PDT process can cause remonomerization, so one cannot completely ignore the nonmonomeric forms.[27]

Analysis of the line shape of the AlS_2Pc absorption peak *in vivo* showed it to be composed of two spectral components, one blue-shifted by 0−5 nm and one red-shifted by 12−15 nm from the spectral locations of the single peak of AlS_2Pc seen in aqueous solution. The 0−5 nm blue-shifted component is very similar to the AlS_2Pc spectrum we see in a cuvette for an aqueous solution (where small shifts can be induced by different saline and pH environments). The component that is red-shifted is consistent with a similar shift seen by previous workers in murine blood.[25,28] This points to the drug existing in two distinct chemical environments, and passing from the red-shifted to the slightly blue-shifted compartment between the 1 and 24 h measurements (the red-shifted peak is much more dominant at the 1 h time point in all organs except for the liver). However, there are a number of factors pointing to this effect not being solely due to localization of AlS_2Pc in blood: a phantom that utilized whole blood exhibited no red-shifted component (not shown); and previous workers saw only small red shifts when adding an excess of human serum albumin to phthalocyanine in solution.[29] In work carried out on murine ascites, a concentration-dependent red shift was seen, which was attributed to binding to nonspecific biological substrates.[25] It was noted that intracellular AlS_2Pc does not show a spectral shift of this nature, although encapsulation in lysosomes significantly increases the local concentration, creating dimerized species.[30] This compartmentalization measurement offers a promising future avenue for research, especially in the field of Photochemical Internalization.[27]

5. Conclusions

In conclusion, OP shows promise for measuring tissue concentration of photosensitizers in real time and so for better real-time prediction of the extent of necrosis in photodynamic therapy.

Acknowledgments

We thank Dr Stephen Chad Kanick and Dr Robert Parker of the University of Pittsburgh for discussions regarding analytical approaches. The US Department of Health and Human Services National Institutes of Health (NIH) are gratefully acknowledged for their funding of this project (project No. 5 U54 CA 104677-05), which was part of the NTROI programme (Network for Translational Research on Optical Imaging). This work was undertaken at UCLH/UCL who received a proportion of funding from the Department of Health's NIHR Biomedical Research Centres funding scheme. The views expressed in this publication are those of the authors and not necessarily those of the Department of Health. This work was supported by the Experimental Cancer Medicine Centre, University College London.

References

1. J. R. Mourant, T. M. Johnson, G. Los, I. J. Bigio, "Non-invasive measurement of chemotherapy drug concentrations in tissue: Preliminary demonstrations of *in vivo* measurements," *Phys. Med. Biol.* **44**, 1397−1417 (1999).
2. S. C. Kanick, J. L. Eiseman, R. S. Parker, "Pharmacokinetic modeling of motexafin gadolinium disposition in mouse tissues using optical pharmacokinetic system measurements," *Photodiagnosis. Photodyn. Ther.* **5**, 276−284 (2008).

3. A. Johansson, J. Svensson, N. Bendsoe, K. Svanberg, E. Alexandratou, M. Kyriazi, D. Yova, S. Grafe, T. Trebst, S. Andersson-Engels, "Fluorescence and absorption assessment of a lipid mTHPC formulation following topical application in a non-melanotic skin tumor model," *J. Biomed. Opt.* **12**, 034026 (2007).
4. K. S. Johnson, D. W. Chicken, D. C. Pickard, A. C. Lee, G. Briggs, M. Falzon, I. J. Bigio, M. R. Keshtgar, S. G. Bown, "Elastic scattering spectroscopy for intraoperative determination of sentinel lymph node status in the breast," *J. Biomed. Opt.* **9**, 1122−1128 (2004).
5. L. B. Lovat, K. Johnson, G. D. Mackenzie, B. R. Clark, M. R. Novelli, S. Davies, M. O'Donovan, C. Selvasekar, S. M. Thorpe, D. Pickard, R. Fitzgerald, T. Fearn, I. J. Bigio, S. G. Bown, "Elastic scattering spectroscopy accurately detects high grade dysplasia and cancer in Barrett's oesophagus," *Gut* **55**, 1078−1083 (2006).
6. A. Sharwani, W. Jerjes, V. Salih, B. Swinson, I. J. Bigio, M. El-Maaytah, C. Hopper, "Assessment of oral premalignancy using elastic scattering spectroscopy," *Oral Oncol.* **42**, 343−349 (2006).
7. R. Reif, O. A'amar, I. J. Bigio, "Analytical model of light reflectance for extraction of the optical properties in small volumes of turbid media," *Appl. Opt.* **46**, 7317−7328 (2007).
8. R. A. Weersink, J. E. Hayward, K. R. Diamond, M. S. Patterson, "Accuracy of noninvasive *in vivo* measurements of photosensitizer uptake based on a diffusion model of reflectance spectroscopy," *Photochem. Photobiol.* **66**, 326−335 (1997).
9. A. Kienle, M. S. Patterson, "Improved solutions of the steady-state and the time-resolved diffusion equations for reflectance from a semi-infinite turbid medium," *J. Opt. Soc. Am. A Opt. Image Sci. Vis.* **14**, 246−254 (1997).
10. R. M. Doornbos, R. Lang, M. C. Aalders, F. W. Cross, H. J. Sterenborg, "The determination of *in vivo* human tissue optical properties and absolute chromophore concentrations using spatially resolved steady-state diffuse reflectance spectroscopy," *Phys. Med. Biol.* **44**, 967−981 (1999).
11. J. R. Mourant, I. J. Bigio, D. A. Jack, T. M. Johnson, H. D. Miller, "Measuring absorption coefficients in small volumes of highly scattering media: Source-detector separations for which path lengths do not depend on scattering properties," *Appl. Opt.* **36**, 5655−5661 (1997).
12. T. J. Dougherty, C. J. Gomer, B. W. Henderson, G. Jori, D. Kessel, M. Korbelik, J. Moan, Q. Peng, "Photodynamic therapy," *J. Natl. Cancer Inst.* **90**, 889−905 (1998).
13. H. U. Ahmed, D. Pendse, R. Illing, C. Allen, J. H. van der Meulen, M. Emberton, "Will focal therapy become a standard of care for men with localized prostate cancer?," *Nat. Clin. Pract. Oncol.* **4**, 632−642 (2007).
14. L. Ayaru, J. Wittmann, A. J. Macrobert, M. Novelli, S. G. Bown, S. P. Pereira, "Photodynamic therapy using verteporfin photosensitization in the pancreas and surrounding tissues in the Syrian golden hamster," *Pancreatology* **7**, 20−27 (2007).
15. H. R. Jager, M. N. Taylor, T. Theodossy, C. Hopper, "MR imaging-guided interstitial photodynamic laser therapy for advanced head and neck tumors," *AJNR Am. J. Neuroradiol.* **26**, 1193−1200 (2005).
16. S. P. Pereira, L. Ayaru, A. Rogowska, A. Mosse, A. R. Hatfield, S. G. Bown, "Photodynamic therapy of malignant biliary structures using meso-tetrahydroxyphenylchlorin," *Eur. J. Gastroenterol. Hepatol.* **19**, 479−485 (2007).
17. M. Zellweger, P. Grosjean, P. Monnier, H. van den Bergh, G. Wagnieres, "Stability of the fluorescence measurement of Foscan in the normal human oral cavity as an indicator of its content in early cancers of the esophagus and the bronchi," *Photochem. Photobiol.* **69**, 605−610 (1999).
18. D. Phillips, D. Dhami, R. Ostler, Z. Petrasek, "The dimerisation of phthalocyanines," *Progress in Reaction Kinetics and Mechanism* **28**, 299−420 (2003).
19. P. T. Chatlani, P. J. Nuutinen, N. Toda, H. Barr, A. J. Macrobert, J. Bedwell, S. G. Bown, "Selective necrosis in hamster pancreatic tumours using photodynamic therapy with phthalocyanine photosensitisation," *Br. J. Surg.* **79**, 786−790 (1992).
20. J. H. Woodhams, L. Kunz, S. G. Bown, A. J. Macrobert, "Correlation of real-time haemoglobin oxygen saturation monitoring during photodynamic therapy with microvascular effects and tissue necrosis in normal rat liver," *Br. J. Cancer* **91**, 788−794 (2004).
21. T. K. Lee, E. D. Baron, T. H. Foster, "Monitoring Pc 4 photodynamic therapy in clinical trials of cutaneous T-cell lymphoma using noninvasive spectroscopy," *J. Biomed. Opt.* **13**, 030507 (2008).
22. C. J. Tralau, H. Barr, D. R. Sandeman, T. Barton, M. R. Lewin, S. G. Bown, "Aluminum sulfonated phthalocyanine distribution in rodent tumors of the colon, brain and pancreas," *Photochem. Photobiol.* **46**, 777−781 (1987).
23. H. Barr, C. J. Tralau, A. J. Macrobert, N. Krasner, P. B. Boulos, C. G. Clark, S. G. Bown, "Photodynamic therapy in the normal rat colon with phthalocyanine sensitisation," *Br. J. Cancer* **56**, 111−118 (1987).

24. S. A. Prahl, "Hemoglobin spectra," *Oregon Medical Laser Center, Oregon, USA* (1999).
25. A. J. Welch and M. J. van Gemert, *Optical-Thermal Response of Laser-Irradiated Tissue*, Plenum, 2005.
26. S. Kascakova, B. Kruijt, H. S. de Bruijn, van der Ploeg-van den Heuvel , D. J. Robinson, H. J. Sterenborg, A. Amelink, "*Ex vivo* quantification of mTHPC concentration in tissue: Influence of chemical extraction on the optical properties," *J. Photochem. Photobiol. B* **91**, 99−107 (2008).
27. K. Berg, J. C. Bommer, J. Moan, "Evaluation of sulfonated aluminum phthalocyanines for use in photochemotherapy. A study on the relative efficiencies of photoinactivation," *Photochem. Photobiol.* **49**, 587−594 (1989).
28. R. Cubeddu, G. Canti, M. Musolino, A. Pifferi, P. Taroni, G. Valentini, "*In vivo* absorption spectrum of disulphonated aluminium phthalocyanine in a murine tumour model," *J. Photochem. Photobiol. B* **34**, 229−235 (1996).
29. L. Kunz, J. P. Connelly, J. H. Woodhams, A. J. Macrobert, "Photodynamic modification of disulfonated aluminium phthalocyanine fluorescence in a macrophage cell line," *Photochem. Photobiol. Sci.* **6**, 940−948 (2007).
30. P. Taroni, A. Pifferi, A. Torricelli, D. Comelli, R. Cubeddu, "*In vivo* absorption and scattering spectroscopy of biological tissues," *Photochem. Photobiol. Sci.* **2**, 124−129 (2003).